IEEE Photonics Journal
An IEEE Photonics Society Publication

Two-Mode Waveguide Characterization by Intensity Measurements from Exit Face Images

Volume 4, Number 1, February 2012

Xesús Prieto-Blanco
Jesús Liñares

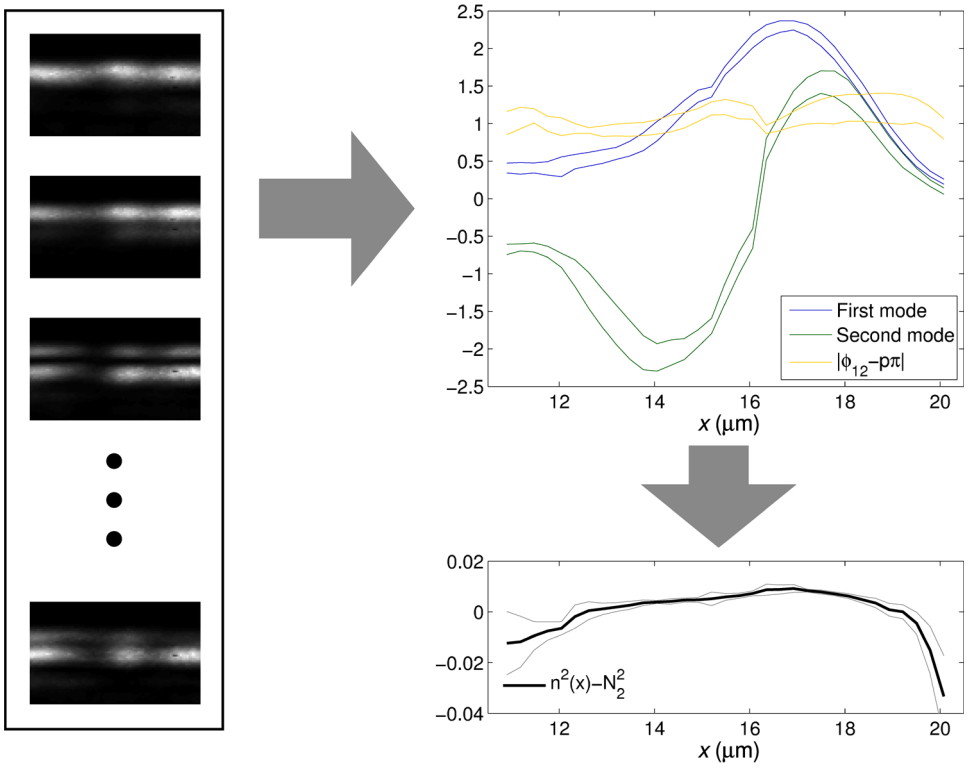

DOI: 10.1109/JPHOT.2011.2177516
1943-0655/$26.00 ©2011 IEEE

IEEE photonics SOCIETY

IEEE

Two-Mode Waveguide Characterization by Intensity Measurements from Exit Face Images

Xesús Prieto-Blanco and Jesús Liñares

Departamento de Física Aplicada, Área de Óptica, Escola Universitaria de Óptica e Optometría, Campus Vida, Universidade de Santiago de Compostela, 15782 Galicia, Spain

DOI: 10.1109/JPHOT.2011.2177516
1943-0655/$26.00 ©2011 IEEE

Manuscript received October 11, 2011; revised November 15, 2011; accepted November 18, 2011. Date of publication December 6, 2011; date of current version December 30, 2011. Corresponding author: X. Prieto-Blanco (e-mail: xesus.prieto.blanco@usc.es).

Abstract: A method that characterizes two-mode waveguides whose modes cannot be selectively excited (such as buried waveguides) is presented and demonstrated. The theoretical results are presented for *N* modes, although for the sake of simplicity, only the two-mode case is developed. The values of the optical mode fields are recovered from several images of the waveguide exit face, where both modes interfere with different relative intensity in each image. From these mode fields, both the squared index distribution, except in an additive constant, and the effective index difference can be obtained by inverting the Helmholtz equation. As in the case of the standard monomode intensity method, the relative values of effective indices and index distributions become absolute if the modes are retrieved in a point of known index, for instance, in the substrate. The method can also be applied to multimode guides if only two modes are excited. In fact, an inexpensive setup is proposed to excite the first two modes of a multimode buried waveguide. This waveguide was fabricated by ion exchange in glass and buried by electromigration. The shape of the squared refractive index recovered by the proposed method agrees with that reported in the literature.

Index Terms: Visible lasers, waveguide devices, waveguide characterization.

1. Introduction

One of the main tasks in integrated optics is the characterization of waveguides. Optical characterization spans a wide range of measurements of waveguide characteristics, such as, for example, refractive index profile, mode effective indices, modal intensities, modal losses, modal dispersion, and so on. Many different characterization methods implemented by diverse techniques have been proposed ever since the beginnings of integrated optics, and they have set down the foundations of many other techniques. Thus, interferometry techniques are among the most used [1]–[6] to measure mainly the refractive index profiles of integrated waveguides, however they used to be very laborious and destructive. Another well-known method of slab waveguide characterization is the *M*-line one, based on the prism-guide coupling technique, to measure the effective indices, and, accordingly, to model the refractive index profile and the optical modes [7], [8]. This method is very useful and powerful when there are several guided modes; however it requires that the integrated guides be found on the surface of the substrate, otherwise (buried guides) the prism-guide coupling technique cannot be applied because the coupling between the guided modes and the prism radiation modes is negligible. An adaptation was also proposed for the measurement of effective indices of surface channel waveguides [9], but the recovery of the 2-D index profile is not obvious.

Another interesting technique of characterization is the measurement of the modal intensity, which allows us to recover the index distribution by inverting the Helmholtz equation. The mode is usually obtained in far-field regime, either from the diffracted modal fields [10] or by imaging the exit face of the guide on an image sensor [11]–[13], although the near field scanning was also used [14]. This technique is particularly useful for monomode guides because their mode can be excited by the end-fire coupling method. For multimode guides we should excite the modes in a selective way, as for example the modes of a surface (nonburied) slab guide which are excited by prism-guide coupling. In other cases, such as optical fibers or buried (channel or slab) guides with two or more modes, the end-fire coupling technique also fails because a selective modal excitation is not possible. In this paper, we focus our attention on this last case, that is, on the buried guides with more than one mode.

We must underline that although the transmission and/or interconnection in integrated optics is usually made in a monomode regime, a recent interest is arising in few-mode fibers to improve the data throughput of monomode fibers [15]. Furthermore, the most of the integrated devices are based on components working at a regime of a few modes. Basic examples of such components are the couplers of two monomode guides or even couplers of one guide with two modes. If these components were buried then the most direct and nondestructive technique of modal characterization would be the direct measurement of simultaneously excited modal fields. In particular, we will analyze a slab buried guide obtained by electric field-assisted ion exchange in glass by using image intensity measurements at the exit face. Since the modes cannot be excited in a selective way, then we will have in each point of the image the interference of the excited modes in the guide. Our method is based on the capture of several images of the waveguide exit plane, each one for a different modal excitation. This allows us to determine the contribution of each mode at each image point and therefore to obtain the values of the modal fields. From these modal fields, the difference between their effective indices and the index profile can also be obtained in the same way as the monomode intensity method. In that sense, our method can be considered as a generalization of the former one. The theoretical results are presented for the case of N modes, although we must underline that the method takes a simple form in the two-mode case $N = 2$ which is developed. Likewise, the results of the two-mode case can be used in multimode guides under particular modal excitation conditions, for instance, a modified end-fire coupling method, which primarily excites the first two modes, is proposed.

The plan of this paper is as follows: In Section 2, we present the main theoretical results for N modes concerning the method of characterization based on the multimode intensity measurements, as well as the main steps of the algorithm to be used in the data processing of the two-mode case. Section 3.1 is devoted to describe the fabrication of a slab buried waveguide by a field-assisted ion-exchange process while the optical setup to perform the intensity measurements is presented in Section 3.2. Section 4 deals with the image intensity data processing when only two modes are excited, and accordingly, the retrieval of the modal amplitude, the relative modal phase, the refractive index profile, and the effective index difference are discussed. Conclusions are given in Section 5.

2. Coupling Theory

In this section, we present the main theoretical results to be used throughout the work. First of all, we deal with the modal coupling problem of an input optical field $\mathbf{E}_i$ into an integrated N-mode waveguide in order to derive a consistent multimode optical intensity function. Next, we present a general method to recover the modal amplitude values (characterization) starting from intensity measurements. Finally, we apply this method to the two-mode case, leading to explicit and, above all, manageable results.

2.1. Multimode Intensity

Let us consider a multimode optical waveguide represented by a refractive index profile $n(x, y)$ and supporting monochromatic guided modes $\boldsymbol{E}_\nu(x, y, z, t)$, $\boldsymbol{H}_\nu(x, y, z, t)$ (in which, for the sake of

simplicity, we choose only a modal subindex ν) propagating along z. These modes can be represented by the following vectorial complex expressions:

$$\boldsymbol{E}_\nu(x,y,z,t) = \mathcal{E}_\nu(x,y,z)\,\mathrm{e}^{-\mathrm{i}\omega t} = \mathbf{E}_\nu(x,y)\,\mathrm{e}^{\mathrm{i}[\beta_\nu z-\omega t]} \tag{1}$$

$$\boldsymbol{H}_\nu(x,y,z,t) = \mathcal{H}_\nu(x,y,z)\,\mathrm{e}^{-\mathrm{i}\omega t} = \mathbf{H}_\nu(x,y)\,\mathrm{e}^{\mathrm{i}[\beta_\nu z-\omega t]} \tag{2}$$

where $\{\mathbf{E}_\nu(x,y), \mathbf{H}_\nu(x,y)\}$ and β_ν are the modal complex vectorial amplitude and the propagation constant of the ν-mode. It must be noted that the transverse and longitudinal modal components are real and imaginary, respectively.

On the other hand, the quasi-complete orthonormalization condition of two modes: ν and ν', on a cross section of an optical guide, is given by the following expression [16], [17]:

$$2\,\mathrm{sgn}_\nu \iint \{\boldsymbol{e}_{\nu'} \wedge \boldsymbol{h}_\nu^\star\}\boldsymbol{u}_z\,dx\,dy = \delta_{|\nu|,|\nu'|} \tag{3}$$

where $\delta_{|\nu|,|\nu'|}$ is the Kronecker delta, the function sgn_ν is defined as $+1$ if $\nu > 0$ (forward modes) and as -1 if $\nu < 0$ (backward modes), and $\boldsymbol{e}_\nu$, $\boldsymbol{h}_\nu$ are the normalized modes, that is, $\boldsymbol{e}_\nu = \mathbf{E}_\nu/\|\mathbf{E}_\nu\|$ and $\boldsymbol{h}_\nu = \mathbf{H}_\nu/\|\mathbf{H}_\nu\|$, with [17]

$$\|\mathbf{E}_\nu\| \equiv \|\mathbf{H}_\nu\| = \left\{2\,\mathrm{sgn}_\nu \iint \{\mathbf{E}_\nu \wedge \mathbf{H}_\nu^\star\}\boldsymbol{u}_z\,dx\,dy\right\}^{1/2} \tag{4}$$

that is, the modal norm. Note that the orthonormalization condition (3) is determined only by the transverse field components of the guided modes and it is a quasi-complete orthonormalization condition since for cases such as $\nu = -\nu'$, (3) is not equal to zero; however, it is an exact expression for copropagating (forward) modes which are considered throughout this work.

It is well known that any optical field can be expressed as a linear superposition of normalized modes, thus the spatial complex amplitude $\{\mathcal{E}, \mathcal{H}\}$ of a forward field at any plane z of the guide can be written by means of forward modes as follows:

$$\mathcal{E}(x,y,z) = \sum_\nu a_\nu\,\boldsymbol{e}_\nu(x,y)\,\mathrm{e}^{\mathrm{i}\beta_\nu z} \quad \mathcal{H}(x,y,z) = \sum_\nu a_\nu\,\boldsymbol{h}_\nu(x,y)\,\mathrm{e}^{\mathrm{i}\beta_\nu z} \tag{5}$$

where

$$a_\nu = 2\iint \{\mathcal{E}(x,y,0) \wedge \boldsymbol{h}_\nu^\star\}\boldsymbol{u}_z\,dx\,dy. \tag{6}$$

Thus, starting from (5) and taking into account the modal normalization condition given by (3), the following expression for the total power $\mathcal{P}$ of the optical field $\mathbf{E}$ is derived:

$$\mathcal{P} = 2\iint \{\mathcal{E} \wedge \mathcal{H}^\star\}\boldsymbol{u}_z\,dx\,dy = \sum_\nu |a_\nu|^2 + \mathcal{P}_r \tag{7}$$

with $|a_\nu|^2$ the power coupled to each guided mode (guided mode power) and where, for the sake of consistency, we have added the power coupled to radiation modes $\mathcal{P}_r$. It would even be necessary to add other powers such as reflection power, absorption power, and so on; therefore, $\mathcal{P}_r$ can also be understood as the contribution of all of them. In Section 2.2, we will take into account these powers $\mathcal{P}_r$ in order to define the power coupled to each mode in a compatible way with the experimental intensity measurements.

On the other hand, we can define the intensity $\mathcal{I}$ of the optical field $\mathcal{E}$ as a function of the amplitudes of the optical modes, that is, the multimode intensity

$$\mathcal{I}(x,y,z) = \{\mathcal{E} \wedge \mathcal{H}^\star\}\boldsymbol{u}_z = \left\{\sum_{\nu,\nu'} a_\nu\,\boldsymbol{e}_\nu(x,y)\,\mathrm{e}^{\mathrm{i}\beta_\nu z} \wedge a_{\nu'}^\star\,\boldsymbol{h}_{\nu'}^\star(x,y)\,\mathrm{e}^{\mathrm{i}\beta_{\nu'} z}\right\}\boldsymbol{u}_z. \tag{8}$$

This equation can be simplified by means of very usual assumptions on modal fields. Thus, in the case of modes of slab guides, that is, with refractive index profile $n(x)$, we can distinguish between TE and TM modes because the TE modes fulfill the relationship: $\beta_\nu \mathrm{E}_{y\nu} = -\omega\mu_o \mathrm{H}_{x\nu}$ and $\mathrm{E}_{x\nu} = 0$ and the TM modes fulfill the relationship: $\beta_\nu \mathrm{H}_{y\nu} = -\omega\mu_o \mathrm{E}_{x\nu}$ and $\mathrm{E}_{y\nu} = 0$. These relationships are quasi-exact for most of the channel waveguides and in particular for those whose width is larger than their height, and therefore these modes are called QTE (quasi-TE) and QTM (quasi-TM) modes.

Note that the expansion coefficients a_ν correspond to the case of an optical field $\mathcal{E}$ inside the guide, however the practical problem always involves the coupling of an input optical field $\mathcal{E}_i$ from, for instance, the vacuum. Therefore, we must slightly change the expansion coefficients, that is, within the paraxial approximation and in a good approximation for an input optical field with plane phase, that is, $\mathcal{E}_i$ a real function at $z = 0$, we can write

$$c_\nu \approx 2 \iint t_\nu \left\{ \mathcal{E}_i(x, y, 0) \wedge \boldsymbol{h}_\nu^\star \right\} \boldsymbol{u}_z \, dx \, dy \tag{9}$$

where $t_\nu = 2N_\nu/(1 + N_\nu)$ are the transmission coefficients for each mode ν which has an effective index N_ν. Thus, taking into account the last relationship and that in most integrated waveguides the effective indices fulfill the relation $N_\nu - N'_\nu \ll N_1$, then (8) can be approximately rewritten as follows:

$$\mathcal{I}(x, y, z) \approx \frac{N_1}{c\mu_o} \left\{ \sum_\nu |c_\nu|^2 e_\nu^2(x, y) + \sum_{\nu \neq \nu'} c_\nu c_{\nu'} \mathrm{e}^{\mathrm{i}\phi_{\nu\nu'}} \, e_\nu(x, y) e_{\nu'}(x, y) \right\} \tag{10}$$

with $\phi_{\nu\nu'} = (\beta_\nu - \beta_{\nu'})z$, $e_\nu \equiv e_{y\nu}$ and, in a good approximation, for calculations concerning the intensity, we have chosen $N_\nu \approx N_1$, $\forall \nu$. Note that all coefficients c_ν are real because t_ν, $h_{y\nu}$, and $\mathcal{E}_i(x, y, 0)$ are also real; therefore, the only complex numbers are the phases $\mathrm{e}^{\mathrm{i}\phi_{\nu\nu'}}$.

2.2. Modal Amplitudes From Intensity Measurements

By taking into account the results of the above subsection, we describe a general procedure to obtain the modal amplitudes starting from measurements of multimode intensity at a plane z of a multimode guide. Let us consider a slab guide, although the results can be extended to channel guides in a straightforward way. Let us consider N modes in a guide; then we perform a first set of measurements of intensity at N points at the exit plane of the waveguide excited by an input real field $\mathcal{E}_i(x, y, 0)$, that is, $(I_e^{(1)}(1), \ldots, I_e^{(1)}(N))$, with subindex e indicating the experimental values; next, we modify the input field, for instance, by shifting it or by changing its size (by image system) but keeping the phase of the input field constant; thus, we obtain a new set of measurement, and we continue until reaching the M-set, that is, $(I_e^{(M)}(1), \ldots, I_e^{(M)}(N))$.

On the other hand, from a theoretical point of view, we have N equations for the modal coupling intensity of the points $j = 1, \ldots, N$, that is

$$\mathcal{I}(j) \approx \frac{N_1}{c\mu_o} \left\{ \sum_\nu |c_\nu|^2 e_\nu^2(j) + \sum_{\nu \neq \nu'} c_\nu c_{\nu'} \mathrm{e}^{\mathrm{i}\phi_{\nu\nu'}} e_\nu(j) e_{\nu'}(j) \right\}. \tag{11}$$

Note that we have N equations and $N - 1$ parameters c_ν because of the condition given by (7) applied to the modal coupling coefficients c_ν, that is, because of the power conservation. Nevertheless, as commented above, there is coupling to the radiation modes, the reflective modes and so on, accordingly we must modify slightly the condition (7) to be compatible with both experimental measurements and with (11), that is, we define new coefficients $\tilde{c}_\nu$ fulfilling

$$\sum_\nu |\tilde{c}_\nu|^2 = \sum_\nu \frac{|c_\nu|^2}{\mathcal{P} - \mathcal{P}_r} = 1 \tag{12}$$

where the factor $\mathcal{P}-\mathcal{P}_r=\mathcal{P}_t$ is nothing but the transmitted power; therefore, by taking into account these new coefficients, we can rewrite (11) as follows:

$$I(j)\approx\sum_{\nu}|\tilde{c}_\nu|^2e_\nu^2(j)+\sum_{\nu\neq\nu'}\tilde{c}_\nu\tilde{c}_{\nu'}e^{i\phi_{\nu\nu'}}e_\nu(j)e_{\nu'}(j) \tag{13}$$

where $I(j)=c\mu_o\mathcal{I}(j)/N_1\mathcal{P}_t$. In short, the above equations define a hypersurface in an abstract N-dimensional space and in a parametric form with $N-1$ free parameters $\tilde{c}_\nu$, that is, all multimode intensity values on the N points are found on a hypersurface whose constant values $e_\nu(j)$ at the N points together with the phases $\phi_{\nu\nu'}$ (which are the same at all points) must be calculated. For that purpose, we must note that such values of the modal amplitudes $e_\nu(j)$ and phases $\phi_{\nu\nu'}$ at N points are those that minimize the distance between the experimental values of the multimode intensity and their respective theoretical values on the hypersurface. If we want to recover more values of the modal amplitudes e_ν we should repeat all the process with N new points, and so forth. Obviously, this is a huge task even from a numerical point of view; however, for two modes (and even for three and four modes), it gives rise to a reasonable volume of calculation, as shown in the next section.

2.3. Modal Amplitudes From Two-Mode Intensity

When we consider only two excited modes, although the guide owns more than two modes, a drastic reduction of calculation time is obtained. Indeed, (11) for two points $j=1,2\ (=u,v)$ and two modes $\nu=1,2$ turn into the following two simple equations of two-mode intensity:

$$\mathcal{I}_u\approx\frac{N_1}{c\mu_o}\left\{|c_1|^2e_{1u}^2+|c_2|^2e_{2u}^2+c_1c_2e^{i\phi_{12}}\,e_{1u}e_{2u}+c.c.\right\} \tag{14}$$

$$\mathcal{I}_v\approx\frac{N_1}{c\mu_o}\left\{|c_1|^2e_{1v}^2+|c_2|^2e_{2v}^2+c_1c_2e^{i\phi_{12}}\,e_{1v}e_{2v}+c.c.\right\}. \tag{15}$$

In this case, the modal intensity equations define a curve on the abstract plane $\mathcal{I}_u-\mathcal{I}_v$ where the values of interest to be determined are e_{1u}, e_{2u}, e_{1v}, and e_{2v}. Next, we must derive the curve defined by the above equations. To this end, and as in the multimode case, by taking into account (12), we write

$$\frac{|c_1|^2}{\mathcal{P}-\mathcal{P}_r}+\frac{|c_2|^2}{\mathcal{P}-\mathcal{P}_r}\equiv|\tilde{c}_1|^2+|\tilde{c}_2|^2=1 \tag{16}$$

therefore, starting from the condition $|\tilde{c}_1|^2+|\tilde{c}_2|^2=1$ we can define $\tilde{c}_1=\cos\alpha$ and $\tilde{c}_2=\sin\alpha$. Next, by taking into account (13), we rewrite (14) and (15) in a parametric way as follows:

$$I_u\approx e_{1u}^2\cos^2\alpha+e_{2u}^2\sin^2\alpha+2e_{1u}e_{2u}\cos\phi_{12}\cos\alpha\sin\alpha \tag{17}$$

$$I_v\approx e_{2v}^2\cos^2\alpha+e_{2v}^2\sin^2\alpha+2e_{1v}e_{2v}\cos\phi_{12}\cos\alpha\sin\alpha. \tag{18}$$

In order to make easier the calculation of the curve defined by the above equations, we introduce the following useful parameters:

$$\bar{I}_j=\frac{e_{1j}^2+e_{2j}^2}{2},\qquad \Delta I_j=\sqrt{\left(\frac{e_{1j}^2-e_{2j}^2}{2}\right)^2+(e_{1j}e_{2j}\cos\phi_{12})^2} \tag{19}$$

$$\varphi=\arctan\frac{2e_{1v}e_{2v}\cos\phi_{12}}{e_{1v}^2-e_{2v}^2}-\arctan\frac{2e_{1u}e_{2u}\cos\phi_{12}}{e_{1u}^2-e_{2u}^2}. \tag{20}$$

Next, after a long but straightforward calculation, we obtain the following implicit equation:

$$\left(\frac{I_u-\bar{I}_u}{\Delta I_u}\right)^2+\left(\frac{I_v-\bar{I}_v}{\Delta I_v}\right)^2-2\frac{I_u-\bar{I}_u}{\Delta I_u}\frac{I_v-\bar{I}_v}{\Delta I_v}\cos\varphi=\sin^2\varphi. \tag{21}$$

This equation states that the normalized intensities I_u and I_v at any two points of a two-mode waveguide are correlated. In particular, we have obtained an ellipse centered on the point $(\bar{I}_u,\bar{I}_v)$ of the plane $I_u - I_v$. This ellipse is inscribed in a rectangle with sides ΔI_u and ΔI_u, and rotated an angle Ψ given by the expression

$$\tan 2\Psi = 2\frac{\Delta I_u \Delta I_v}{(\Delta I_u)^2 - (\Delta I_v)^2}\cos\varphi. \tag{22}$$

By taking into account (21), a few useful remarks can be made. The horizontal coordinate of the ellipse center $(\bar{I}_u)$ is small only if the modal amplitudes of the point u are small, that is, in the mode tails. Likewise, the horizontal half size of the ellipse (ΔI_u) must be always smaller than $\bar{I}_u$ to preserve $I_u > 0$. Besides, ΔI_u cancels only if the relative phase of the two modes (ϕ_{12}) is $\pi/2$ and its amplitudes take the same value at the point u. Similarly, the mode amplitudes at the waveguide point v set the vertical position and the size of the circumscribing rectangle. If the points u and v are near each other, their modal amplitudes are similar, φ is small and the ellipse comes close to a diagonal of the rectangle. Inversely, the ellipse is referred to its axes when φ is equal to $\pi/2$. For example, if v is a point where the first and the second modal amplitudes are equal $(e_{1v} = e_{2v})$ and u is at the node of the second mode $(e_{2u} = 0)$, then $\varphi = \pi/2$, as seen in (20).

After M measurements at the selected two points, that is, $\{(I_{eu}^{(1)}, I_{ev}^{(1)}), \ldots, (I_{eu}^{(M)}, I_{ev}^{(M)})\}$, we must find the best fitting of these points to an ellipse in the abstract space $I_u - I_v$. We need at least five points in that space to obtain the above five parameters, that is, five different input fields are indispensable $(M \geq 5)$, although much more of them are desirable. The improvement given in [18] about the algorithm of Fitzgibbon *et al.* [19] is used to carry out the fitting. This algorithm is very appropriate because it is linear, fast, simple to implement and moreover specific to ellipses (parabolas or hyperbolas are never obtained). This algorithm returns the parameters $\hat{a}$, $\hat{b}$, $\hat{c}$, $\hat{d}$, $\hat{e}$, and $\hat{f}$ of the following equation:

$$\hat{a}I_u^2 + \hat{b}I_uI_v + \hat{c}I_v^2 + \hat{d}I_u + \hat{e}I_v + \hat{f} = 0.$$

We need to relate the parameters of the above equation with the parameters $\bar{I}_u, \bar{I}_v$, ΔI_u, ΔI_v, and φ of (21); after some algebra, the following is obtained

$$\bar{I}_u = \frac{\hat{b}\hat{e} - 2\hat{c}\hat{d}}{4\hat{a}\hat{c} - \hat{b}^2}, \qquad \Delta I_u = 2\sqrt{\hat{c}}\frac{\sqrt{\hat{a}\hat{e}^2 + \hat{c}\hat{d}^2 - \hat{b}\hat{d}\hat{e} - (4\hat{a}\hat{c} - \hat{b}^2)\hat{f}}}{4\hat{a}\,\hat{c} - \hat{b}^2}$$

$$\bar{I}_v = \frac{\hat{b}\hat{d} - 2\hat{a}\hat{e}}{4\hat{a}\hat{c} - \hat{b}^2}, \qquad \Delta I_v = 2\sqrt{\hat{a}}\frac{\sqrt{\hat{a}\hat{e}^2 + \hat{c}\hat{d}^2 - \hat{b}\hat{d}\hat{e} - (4\hat{a}\hat{c} - \hat{b}^2)\hat{f}}}{4\hat{a}\hat{c} - \hat{b}^2}, \qquad \cos\varphi = -\frac{\hat{b}}{2\sqrt{\hat{a}\hat{c}}}.$$

Next, we define new parameters γ_u and γ_v in order to invert (19) and (20), that is

$$\cos\gamma_u = \frac{\Delta I_u}{\bar{I}_u} \quad \cos\gamma_v = \frac{\Delta I_v}{\bar{I}_v}.$$

Therefore, the phase and modal amplitudes $\tan^2\phi_{12}$, e_{1u}, e_{2u}, e_{1v}, and e_{2v} can be expressed as follows:

$$\tan^2\phi_{12} = \frac{\tan^2\gamma_u + \tan^2\gamma_v - 2\tan\gamma_u\tan\gamma_v\cos\varphi}{\sin^2\varphi} \tag{23}$$

$$e_{\nu u} = \sqrt{\bar{I}_u\left(1 - (-1)^\nu\sqrt{\cos^2\gamma_u - \frac{\sin^2\gamma_u}{\tan^2\phi_{12}}}\right)}, \quad e_{\nu v} = \sqrt{\bar{I}_v\left(1 - (-1)^\nu\sqrt{\cos^2\gamma_v - \frac{\sin^2\gamma_v}{\tan^2\phi_{12}}}\right)}.$$

We must stress that this procedure can also be applied to guides with more than two modes if only two modes are excited simultaneously. For instance, in the case of a three-mode symmetric

TABLE 1

Effective indices after first ion-exchange

	mode 1	mode 2
TE	1.5463	1.5110
TM	1.5448	1.5103

guide, we could excite the first and the third mode by using symmetric input fields of variable width or shape in order to achieve the M measurements.

3. Experimental Implementation

3.1. Slab Buried Waveguide Fabrication

A standard microscope slide (1-mm-thick piece of soda-lime glass) was immersed in a mixture of molten salts. The selected salt composition was: 47.5 mol% $NaNO_3$, 47.5 mol% KNO_3, and 5 mol% $AgNO_3$, since it presents a melting point of 220 °C [20], which allows us to use a diffusion temperature as low as 240 °C. Under these ion-exchange conditions only two modes are obtained after 24 min of diffusion (see Table 1). As this waveguide is a surface slab one, its effective indices were measured by prism coupling method with a Model 2010 prism coupler from Metricon. A simple sodium/silver salt would require too short diffusion time for the same penetration depth of silver cations. We must note that the K^+ cations did not influence the waveguide formation because they have a much lower tendency to enter into the glass than Ag^+ cations. A second diffusion step was carried out to bury this waveguide some micrometers under the glass surface. The sample was placed in a quartz support that allowed us to put in contact each sample side with its respective molten salt at a different electrical potential. In order to remove silver cations from the surface, a 50 mol% $NaNO_3$: 50 mol% KNO_3 salt composition at 272 °C was used as anode in contact with the guiding surface. However, a 50 mol% $AgNO_3$: 50 mol% KNO_3 salt mixture was used as cathode. This silver/potassium composition is nearly eutectic, with the melting point lower than 160 °C [20]; a good electric contact is achieved at the cathode when this salt melts. Initially, the sample was immersed for 10 min without current flow; next, a potential difference of 155 V was applied for 30 min to perform a field-assisted diffusion. However, it is interesting to underline that, since the anode and cathode salts have different composition, an effective potential actually occurs, which can be different from the applied one by some Volt [21]. Once the field-assisted diffusion process was finished, a 7.02-mm-long piece of sample was prepared by cutting and polishing two faces perpendicular to the waveguide and parallel to each other.

3.2. Optical Setup

The optical setup is prepared for illuminating one polished face of the sample (input face defined by $z = 0$) with a cylindrical focused beam whose focal line is parallel to the waveguide (Y axis). In this way, only two modes (as shown later) of the waveguide are excited, and they propagate to the other face (end face). Moreover, the setup contains a microscope objective which forms an image of the end face of the waveguide on a CCD camera to obtain the intensity profile resulting from the interference between both modes.

As the input beam profile is a Gaussian one along the confinement direction of the waveguide (vertical or X axis), and it is collimated along the perpendicular direction, the phase is uniform at the waist plane, where the input face is. It ensures that both modes have the same phase at the input face (except in a π relative phase), irrespective of the height of the beam center or the size of the waist, and therefore, their phase difference at the end face takes always the same value. A variation of the coupling coefficient to each mode is needed in order to apply the algorithm presented in Section 2. A relative vertical shift between the illumination system and the rest of the optical system (sample, imaging objective and CCD) could be an effective way to achieve such variations, but this requires a big stage with submicron resolution. A more cheap and convenient solution that performs the same task is sketched in Fig. 1.

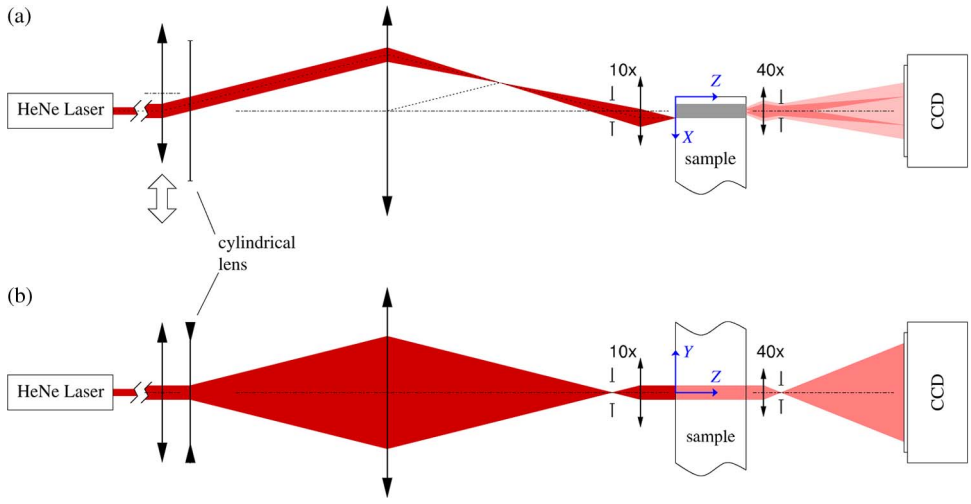

Fig. 1. Simplified diagram of the optical setup.

First, let us see Fig. 1(a), which shows a vertical section of the system. A He-Ne laser beam is refracted through a low-power positive lens (0.5 diopter) that can be moved up and down to redirect the beam with a negligible change in its original divergence. The following lens is a negative cylindrical one with its power meridian along the horizontal axis; therefore, it does not affect the rays of the vertical section. Next, a high-power positive lens (10 diopter) focuses the rays contained in the vertical plane and projects an image of the low-power lens on the back focal plane of a finite-conjugated (DIN standard) 10$\times$ microscope objective. The distances between lenses were arranged in such a way that this image was 160 mm apart from the beam focus. Thus, the objective focuses a high-quality beam again. To place just the input face on the beam waist, the back-reflected beam from this face must maintain the same transversal size as the incident beam along the illumination system. Besides, to ensure that the beam initially falls on the waveguide, its output face is illuminated with a retractable white LED; therefore, both the laser back-reflection (suitably attenuated) and the input face are simultaneously seen through the 10$\times$ microscope objective using a cube beam-splitter placed between the high power positive lens and an eyepiece (not shown in Fig. 1). This illumination system allows us a great control of the beam height since a macroscopical rise (1 mm) of only one element (the first low-power lens) generates a microscopical beam drop at the input face (5 μm). Note that the central ray of this beam is kept parallel to the optical axis; then, its phase is constant along the input face.

If the beam waist at the input face is fitted to the mode size, the beam matches the fundamental mode very well for a particular beam height. In this way, the best coupling coefficient to the first mode is achieved, while the excitation of the second and third mode becomes negligible. A small beam shift from this position increases mainly the coupling coefficient to the second mode (at the expense of the fundamental one) but retains a negligible third mode excitation under moderate shifts. Consequently, only two modes are involved within an interval. As the required waist is wider than the objective resolution, the Gaussian beam must illuminate only a portion of the objective aperture stop. The appropriate expansion of the beam was obtained by taking advantage of its own divergence under a particular propagation distance from the laser to the first lens.

On the other hand, in Fig. 1(b), a projection on the horizontal plane of the beam as it propagates through the system is shown. The main difference with respect to the vertical section is the presence of the power meridian of the cylindrical lens whose axial position was fitted to obtain a horizontally collimated beam at the waveguide input face.

In short, the illumination system generates a high-quality cylindrical beam with its focal line on the input face of the waveguide and parallel to it. Moreover, the beam can be finely moved along the perpendicular direction to moderately change the coupling efficiencies to the first and second mode.

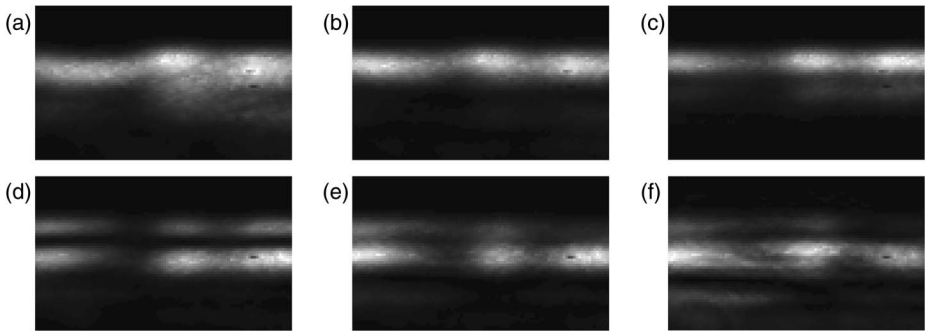

Fig. 2. Some irradiance distributions at a selected region of the end face of the waveguide. The images in (a) and (f) were discarded for processing. In these images, the *X* axis is upwards, while the *Y* axis is horizontal.

The end face was imaged with a standard 40× microscope objective on to an analog Pulnix TM-765 CCD camera, and the signal was digitized to a frame of 767 × 575 pixels and an 8-bit depth by an acquisition board. For each particular beam height, the intensity was adjusted by a set of attenuators, both to achieve a good illumination and to prevent saturation. Then, 256 images were captured and averaged to improve the signal-to-noise ratio (SNR). Next, the beam was vertically shifted 0.5 μm, the intensity was adjusted again, a new averaged image was captured, and so on. Moreover, an averaged final image was taken with the laser obstructed; this final image was subtracted to the previous ones to remove both the background and the camera dark current. In this way, a series of 37 irradiance distributions at the end face was obtained. Some representatives of such distributions are shown in Fig. 2.

4. Image Processing and Results

4.1. Mode Amplitudes

The proprietary software MATLAB was used to apply the algorithm of Section 2 to these images, although the free software Octave could have also been used. The first task is the selection of the region of interest in the images which contains 100 × 60 pixels. Ideally, as the intensity profile should not depend on the *y* coordinate, each image could have been collapsed to a function by averaging it along this dimension, resulting in a new SNR improvement. Actually, a smooth variation can be seen along the *y* dimension, probably due to some lack of uniformity in the waveguide (see Fig. 2). For this reason, groups of only five contiguous columns were collapsed into a new column by applying a median filter. Thus, most defective pixels caused by dust in the cover plate of the CCD camera are discarded. Note that the discrepancy between columns gives us an idea of the accuracy achieved, since each collapsed column will be processed independently. Next, the mode intensity is normalized along the *x* direction according to (12); that is, every column is divided by the sum of the values of its elements. It results in a series of compacted images of 20 × 60 pixels each. The intensity of a given pixel oscillates along the series. According to the general theory, an ellipse arc must be obtained when the intensity of two pixels is plotted one versus another (Fig. 3). Note that this plot contains as many points as images are in the series. However, only 16 images in the center of the series have suitable values to be fitted to ellipses. Modes other than the first and second were noticeably excited in the rest of images that were discarded. From the five ellipse parameters, the absolute value of each mode amplitude at each pair of points, together with the squared tangent of the relative phase, are calculated. This procedure has two inherent shortcomings: the sign of the second mode is lost and the lowest amplitude is always assigned to the first mode, while the highest one is given to the second mode. *A posteriori*, each amplitude value must be assigned to the right mode and the sign of the second mode must be restored. When the second mode at the point u (v) is negative, γ_u (γ_v) must also be considered negative in (23). The depths

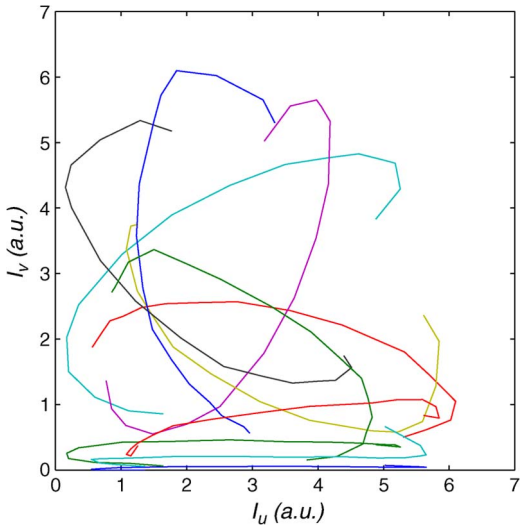

Fig. 3. Experimental normalized intensity of some pairs of points at the waveguide exit face. The intensity of one point (I_v) is graphed against the other (I_u) for several coupling heights of the input beam. The intensities from the same point pair were joined to show their elliptical-like form.

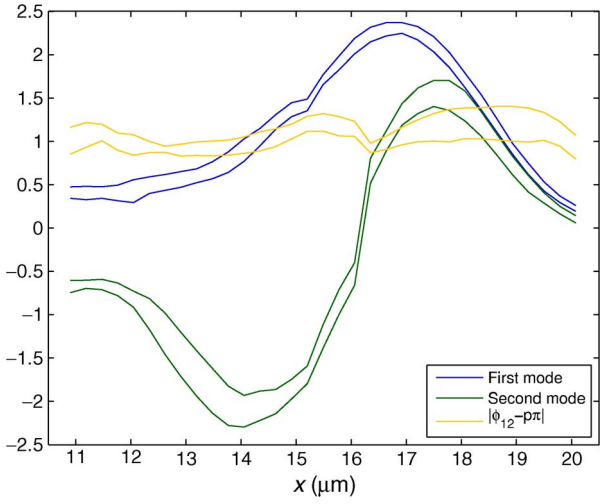

Fig. 4. Retrieved the first and second mode (a.u.) and $|\phi_{12} - p\pi|$ in radians at the output face, where p an unknown integer. Each graph is an average along the slab guide; it is represented by two lines that indicate one standard deviation below and above the mean.

(x values) where both amplitudes meet, or where the second mode cancels, remain the same for every y value, which is an indicator of the consistency of this method.

As the intensities at any pair of points can be fitted to ellipses, all combinations within a given column are checked. Those pairs of points that fit to ellipses which are not fully contained within the first quadrant are discarded, since they provide negative intensities. The modal amplitudes and the phase resulting from the resting pairs are averaged. Thus, 20 profiles (one per column) of the first and second mode are obtained—f_ν—. From their dispersion, we can estimate the uncertainty of the experimental modal amplitudes of both modes—$\sigma_{f_\nu}(x)$—which are shown in Fig. 4. The absolute value of the relative phase between both modes is 1.06 ± 0.17. Likewise, we can check that the modes are approximately orthonormal (see Table 2). However, the point of the second mode closest to its node seems slightly deviated for most of profiles, that is, it contains a bias; therefore, it was removed from subsequent calculations.

TABLE 2

Orthonormality check of the retrieved modes. The values of the table are $(2n_s/c\mu_0)\int f_\nu f_{\nu'}\,dx\,dy$, where ν and ν' are the row and column of the table. The ideal values are indicated in parenthesis

	mode 1	mode 2
mode 1	0.97 (1)	-0.01 (0)
mode 2	-0.01 (0)	0.94 (1)

The left tails of both modes are slightly higher than expected, probably due to a residual excitation of the third mode, which achieves large values in this region. The existence of the third mode is clear in Fig. 2(f), where two intensity minima can be seen.

4.2. Squared Refractive Index Profile

As the experimental modal amplitudes are known, we can retrieve the squared index profile, except an additive constant, starting from the scalar Helmholtz equation, that is

$$n^2(x) - N_\nu^2 = -\frac{1}{k_0^2 e_\nu}\frac{d^2 e_\nu}{dx^2}, \qquad \nu = 1, 2$$

by computing

$$n^2(x) - N_\nu^2 \approx m_\nu(x) \equiv -\left\langle \frac{f_\nu(x-h,y) + f_\nu(x+h,y) - 2f_\nu(x,y)}{f_\nu(x,y)h^2k_0^2} \right\rangle_y \tag{24}$$

where k_0 is the wavenumber, $f_\nu(x,y)$ are the experimental modal amplitudes, h is the step to obtain the second derivative, and the symbol $\langle\ \rangle_y$ means an average along y direction. This calculation must be made carefully since the experimental modal amplitudes contain noticeable noise, that is

$$f_\nu(x,y) = e_\nu(x) + O(\sigma_{f_\nu}(x))$$

where $\sigma_{f_\nu}^2(x)$ are the variances of $f_\nu(x,y)$. On the one hand, since the second derivative [denoted as $f_\nu''(x,y)$] is computed by a typical finite difference scheme, two sources of uncertainty arise: one from the noise and another from the discretization; specifically

$$f_\nu''(x,y) \equiv \frac{f_\nu(x-h,y) + f_\nu(x+h,y) - 2f_\nu(x,y)}{h^2} = \frac{e_\nu(x-h) + e_\nu(x+h) - 2e_\nu(x)}{h^2} + O\left(\frac{4\sigma_{f_\nu}(x)}{h^2}\right)$$
$$= \frac{d^2 e_\nu}{dx^2} + O\left(h^2\frac{d^4 e_\nu}{dx^4}\right) + O\left(\frac{4\sigma_{f_\nu}(x)}{h^2}\right).$$

The last line of this equation shows that very small or very high value of h gives rise to high errors. In our case, a good balance was achieved when h is equal to four pixels, although a three-pixel step was used sometimes to prevent the use of the discarded point. Moreover, a linear variation of the second derivative along x of f_ν was assumed at both the end points and its neighbors.

On the other hand, low values of f_ν have high relative uncertainty which leads to remarkable errors in specific regions when computing $n^2(x) - N_\nu^2$ by (24). In other words, if the variance of $m_\nu(x)$ is calculated as

$$\sigma_{m_\nu}^2(x) = \frac{n_y}{n_y - 1}\left[\left\langle\left(\frac{f_\nu''(x,y)}{f_\nu(x,y)k_0^2}\right)^2\right\rangle_y - m_\nu^2(x)\right]$$

where $n_y = 20$ is the number of compacted columns, the standard deviations $\sigma_{m_\nu}(x)$ are noticeably dependent on x, as can be seen in Fig 5(a). Fortunately, regions of high values of $\sigma_{m_1}^2$ and $\sigma_{m_2}^2$ only overlap at the far tails since the mode orthogonality constrains the node of the second mode near the maximum of the first mode, and conversely, the left tail of the first mode starts where the second mode still takes high values. This fact suggests to combine information from both modes to

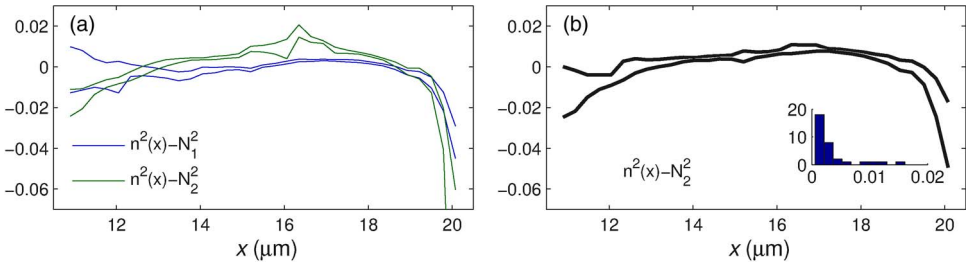

Fig. 5. (a) Squared refractive index profile retrieved from the first (blue) and second mode (green). Each graph is an average along the slab guide; it is represented with two lines that indicate one standard deviation below and above the mean. (b) Combination of such profiles by a weighted average, represented in the same way; a histogram of its standard deviation is shown in the inset (number of points against standard deviation).

construct the refractive index profile more accurately. However, the profiles obtained from each mode differ in a constant $N_1^2 - N_2^2$ that must be calculated previously. This constant was computed as a weighted mean difference between both profiles; the weight must be high only where both profiles have low variance. Therefore, we choose as weight $1/(\sigma^2_{m_1}(x) + \sigma^2_{m_2}(x))$, which leads to

$$N_1^2 - N_2^2 \simeq \delta m \equiv \frac{\sum_x \frac{m_2(x) - m_1(x)}{\sigma^2_{m_1}(x) + \sigma^2_{m_2}(x)}}{\sum_x \frac{1}{\sigma^2_{m_1}(x) + \sigma^2_{m_2}(x)}}.$$

A value of $(514 \pm 26) \cdot 10^{-5}$ was obtained for $N_1^2 - N_2^2$. Once δm is known, the final squared index profile can be obtained as a weighted mean of both profiles, but now, the weight of each one is inversely proportional to its variance

$$n^2(x) - N_2^2 \simeq \frac{\frac{m_1(x) + \delta m}{\sigma^2_{m_1}(x)} + \frac{m_2(x)}{\sigma^2_{m_2}(x)}}{\frac{1}{\sigma^2_{m_1}(x)} + \frac{1}{\sigma^2_{m_2}(x)}}.$$

The resulting profile is shown in Fig. 5(b). As expected, the standard deviation of $n^2(x) - N_2^2$ keeps low or moderate for a wide central region and increases strongly in few points at both ends. Specifically, half of the points have a standard deviation of $n(x) - N_2 \simeq (n^2(x) - N_2^2)/(2N_1)$ between $2 \cdot 10^{-4}$ and $6 \cdot 10^{-4}$; and it keeps below $2 \cdot 10^{-3}$ in the 88% of the points. For comparison, the refractive index accuracies of the interferometric methods are $2 \cdot 10^{-3}$ in [2] or $5 \cdot 10^{-4}$ in [4] at every point of the profile. In respect of the shape, a clear asymmetry of the squared index profile can be seen in Fig. 5(b). The index decreases slowly toward the waveguide surface $(x = 0)$ at the left of the maximum, while the reduction toward the substrate is more abrupt. This result is consistent with the one previously reported for buried waveguides fabricated by field-assisted ion exchange in glass [13], [22].

4.3. Effective Index Difference

A parameter of great importance in devices such as directional couplers or multimode interference (MMI) couplers is the coupling length or alternatively the coupling coefficient. It is well known that its value is directly related to the effective index difference, which can be obtained from δm, that is

$$N_1 - N_2 = \frac{N_1^2 - N_2^2}{N_1 + N_2} \simeq \frac{\delta m}{2n_s} = (170 \pm 13) \cdot 10^{-5} \tag{25}$$

where the effective indices of the denominator were approximated by the substrate index $n_s = 1.5100$. The inaccuracy from this approximation is low for the expected values of N_1 and N_2.

On the other hand, we can improve the above result since we know the propagation distance z, therefore we can relate the phase difference between both modes and the difference of effective

indices as follows:

$$\phi_{12} = \frac{2\pi}{\lambda}(N_1 - N_2)z.$$

If the accuracy of $N_1 - N_2$ allows us to find which quadrant ϕ_{12} is in, a more accurate value of this phase may be derived from its squared tangent provided by the fitting to ellipses. Once ϕ_{12} is improved, $N_1 - N_2$ and the coupling length or the coupling coefficient can be also refined by again applying the last equation. Unfortunately, the variance of ϕ_{12} calculated from the effective index difference exceeds 2π in our case because of the large value of z, and hence, this improvement was not made.

Finally, the values of $N_1 - n_s$ and $N_2 - n_s$ can be obtained from the squared index profile if the tails of each mode could be recovered in the substrate region. This does not happen in our sample, but the step index waveguides are good candidates for that. Provided that n_s is known, we may obtain the effective indices. In this case, the difference $N_1 - N_2$ could also be directly obtained from these values, but probably (25) will be more accurate, mainly if N_1 and N_2 are used to evaluate the denominator.

5. Conclusion and Perspectives

When a waveguide is illuminated with a field with constant phase at the input face that excites N modes, the normalized intensities at N points of its exit face are correlated, that is, there is a constraint between these intensities on a hypersurface in an abstract N-dimensional space, which arises from the interference between the excited modes. This interference is very stable since it takes place after a common path along the waveguide. If only two modes are excited, such a constraint is an ellipse. When the normalized intensity of a point is represented against the one of any other point, then the ellipse is mapped by changing the coupling condition. From the ellipse parameters (center coordinates, height, width and tilt), we can retrieve the squared tangent of the relative phase between both modes as well as the absolute value of their amplitude at the considered two points, although the equations do not indicate which value corresponds to each mode.

By repeating the procedure for different point pairs, it is possible to assign the amplitude values to the right mode and fix the sign, that is, it is possible to reconstruct the amplitude of both modes. The self-consistence of the results can be checked in several ways: ellipses fully contained in the first quadrant, redundancy in both the relative phase and the amplitudes from the multiple way to select the point pairs, orthogonality of the final modes or fulfilling some symmetry of the waveguide, etc. Once the modes are obtained, the difference of effective indices and the squared refractive index profile, except an additive constant, can be also retrieved. Moreover, both the index profile and the effective indices may be obtained without ambiguity in those cases in which the retrieved mode tails reach the substrate region.

The proposed method was successfully applied to a buried slab waveguide fabricated by field-assisted ion exchange in glass. Since this guide is multimode (actually a few modes), an optical system to excite almost exclusively the first two modes with a variable relative efficiency was also proposed. This optical system is simple, inexpensive, and accurate since it makes the most of the reduction that the focusing objective provides. The shape of the index profile agrees with that obtained in similar waveguides from other methods previously reported.

Since each mode is extracted from two-mode interferences, the proposed method can be considered as an extension (essentially a preliminary step) of the monomode intensity method to multimode buried waveguides in which the prism-coupling method is not possible. Therefore, our method is an alternative to interferometric methods, although a comparison is not simple. Interferometric methods provide the index profile in a wide region with a uniform accuracy that depends strongly on the system geometry, but the sample preparation is destructive and very time-consuming. On the other hand, our two-mode intensity method is restricted to the waveguide region but has a good repeatability for the most part (between $2 \cdot 10^{-4}$ and $6 \cdot 10^{-4}$ in half of the points). Moreover,

we should stress that it also provides the mode profiles and the mode effective indices or, at least, their difference ($\pm 13 \cdot 10^{-5}$), and this information is of great importance in many cases.

The coupling to the third mode was a limitation in recovering the first and second modes, and therefore, we expect better results in two-mode guides. For instance, monomode dielectric guides at 1.31 or 1.55 μm could be characterized as two-mode guides within the red wavelength range or at least below 1000 nm, provided that the dispersion is known. This could allow the use of common silicon-based cameras whose technology is more mature than that of infrared cameras. Similarly, optical elements for visible spectrum are much more common than infrared optics.

The diffraction is another limit of the proposed setup, which is especially relevant when the mode size is smaller than a wavelength, for instance, in some silicon waveguides. The diffraction limit can be circumvented by a near-field scanning technique, in the same way that some versions of the monomode intensity method do.

The characterization of few-mode fibers, directional couplers or MMI couplers is a natural application of this method. In the last two cases, the difference of the effective indices is especially useful since it sets the coupling length, which is an important parameter of these devices. Even more, if the propagation distance is moderate, the relative phase between the modes can be obtained without ambiguity from its squared tangent. This will lead to a more accurate value of the coupling length.

In short, there are few methods to characterize multimode buried waveguides, and we have proposed and checked a new method to solve this problem.

References

[1] T. Izawa and H. Nakagome, "Optical waveguide formed by electrically induced migration of ions in glass plates," *Appl. Phys. Lett.*, vol. 21, no. 12, pp. 584–586, Dec. 1972.

[2] M. Sochacka, E. Lopez Lago, and Z. Jaroszewicz, "Refractive-index profiling of planar gradient-index waveguides by phase-measuring microinterferometry," *Appl. Opt.*, vol. 33, no. 16, pp. 3342–3347, Jun. 1994.

[3] P. Mrozek, E. Mrozek, and T. Lukaszewicz, "Determination of refractive index profiles of $Ag^+ - Na^+$ ion-exchange multimode strip waveguides by variable wavefront shear double-refracting interferometry microinterferometry," *Appl. Opt.*, vol. 45, no. 4, pp. 756–763, Feb. 2006.

[4] X. Prieto Blanco, "Interferometric characterization and analysis of silver-exchanged glass waveguides buried by electromigration: Slab, channel and slab-sided channel configurations," *J. Opt. A, Pure Appl. Opt.*, vol. 8, no. 2, pp. 123–133, Feb. 2006.

[5] A. Darudi and S. M. R. Sadat Hosseini, "An interferometric method for refractive index profiling of planar gradient index waveguides," *Opt. Lasers Eng.*, vol. 47, no. 1, pp. 133–138, Jan. 2009.

[6] R. Oven, "Measurement of two dimensional refractive index profiles of channel waveguides using an interferometric technique," *Appl. Opt.*, vol. 48, no. 30, pp. 5704–5712, Oct. 2009.

[7] K. Chiang, "Construction of refractive-index profiles of planar dielectric waveguides from the distribution of effective indexes," *J. Lightwave Technol.*, vol. LT-3, no. 2, pp. 385–391, Apr. 1985.

[8] M. Monir, H. El-Refaei, and D. Khalil, "Single-mode refractive index reconstruction using an NM-line technique," *Fiber Integr. Opt.*, vol. 25, no. 2, pp. 69–74, Apr. 2006.

[9] K. S. Chiang and S. Y. Cheng, "Technique of applying the prism-coupler method for accurate measurement of the effective indices of channel waveguides," *Opt. Eng.*, vol. 47, no. 3, p. 034601, Mar. 2008.

[10] K. Hotate and T. Okoshi, "Measurement of refractive-index profile and transmission characteristics of a single-mode optical fiber from its exit-radiation pattern," *Appl. Opt.*, vol. 18, no. 19, pp. 3265–3271, Oct. 1979.

[11] L. McCaughan and E. E. Bergmann, "Index distribution of optical waveguides from their mode profile," *J. Lightwave Technol.*, vol. LT-1, no. 1, pp. 241–244, Mar. 1983.

[12] M. L. Von Bibra and A. Roberts, "Refractive index reconstruction of graded-index buried channel waveguides from their mode intensities," *J. Lightwave Technol.*, vol. 15, no. 9, pp. 1695–1699, Sep. 1997.

[13] Y.-F. Ma, J. Wei, J.-H. Pei, Z.-H. Kang, Y. Jiang, and J.-Y. Gao, "Construction of refractive-index profile of $Ag^+ - Na^+$ ion-exchange channel waveguide by two-dimensional inverse matrix method," *Rev. Sci. Instrum.*, vol. 79, no. 2, p. 025104, Feb. 2008.

[14] W.-S. Tsai, W.-S. Wang, and P.-K. Wei, "Two-dimensional refractive index profiling by using differential near-field scanning optical microscopy," *Appl. Phys. Lett.*, vol. 91, no. 6, pp. 061123-1–061123-3, Aug. 2007.

[15] E. Ip, N. Bai, Y.-K. Huang, E. Mateo, F. Yaman, M.-J. Li, S. Bickham, S. Ten, J. Liñares, C. Montero, V. Moreno, X. Prieto, V. Tse, K. M. Chung, A. Lau, H.-Y. Tam, C. Lu, Y. Luo, G.-D. Peng, and G. Li, "$88 \times 3 \times 112$-gb/s WDM transmission over 50-km of three-mode fiber with inline multimode fiber amplifier," in *Proc. 37th ECOC Postdeadline Papers*, 2011, pp. 1–3.

[16] H. Kogelnik, "Theory of optical waveguides," in *Guided-Wave Optoelectronics*, T. Tamir, Ed. New York: Springer-Verlag, 1990, pp. 7–87.

[17] J. Liñares and M. C. Nistal, "Quantization of coupled modes propagation in integrated optical waveguides," *J. Modern Opt.*, vol. 50, no. 5, pp. 781–790, May 2003.

[18] R. Halí and J. Flusser, "Numerically stable direct least squares fitting of ellipses," in *Proc. 6th Int. Conf. Central Eur. Comput. Graph. Visual.*, Univ. West Bohemia, Plzen, Czech Republic, 1998, vol. 1, pp. 125–132.
[19] A. Fitzgibbon, M. Pilu, and R. B. Fisher, "Direct least square fitting of ellipses," *IEEE Trans. Pattern Anal. Mach. Intell.*, vol. 21, no. 5, pp. 476–480, May 1999.
[20] J. L. Jackel, "Glass waveguides made using low melting point nitrate mixtures," *Appl. Opt.*, vol. 27, no. 3, pp. 472–475, Feb. 1988.
[21] X. Prieto-Blanco, "Electro-diffusion equations of monovalent cations in glass under charge neutrality approximation for optical waveguide fabrication," *Opt. Mater.*, vol. 31, no. 2, pp. 418–428, Oct.–Dec. 2008.
[22] A. Lupascu, A. Kevorkian, T. Boudet, F. Saint-André, D. Persegol, and M. Levy, "Modeling ion exchange in glass with concentration-dependent diffusion coefficients and mobilities," *Opt. Eng.*, vol. 35, no. 6, pp. 1603–1610, Jun. 1996.